

**OPTIMIZATION OF FRACTIONAL-SLOT  
PERMANENT MAGNET SYNCHRONOUS  
MACHINE USING ANALYTICAL SUB-DOMAIN  
MODEL AND DIFFERENTIAL EVOLUTION**

**MOHD REZAL MOHAMED**

**UNIVERSITI SAINS MALAYSIA**

**2019**

**OPTIMIZATION OF FRACTIONAL-SLOT PERMANENT MAGNET  
SYNCHRONOUS MACHINE USING ANALYTICAL SUB-DOMAIN MODEL  
AND DIFFERENTIAL EVOLUTION**

**by**

**MOHD REZAL MOHAMED**

**Thesis submitted in fulfilment of the**

**requirements for the degree of**

**Doctor of Philosophy**

**August 2019**

## ACKNOWLEDGEMENT

First and foremost, I wish to express my gratitude to Associate Professor Ir. Dr. Dahaman Ishak for his guidance and support, without which I would not be able to achieve this milestone. I am very blessed to have the pride and privilege to conduct this investigation under his supervision. His valuable commentary, insightful technical feedback, and continuous encouragement have brought me to the completion of my PhD research. I am also thankful to have a mentor with compassion, friendship, and a great sense of humour. I am grateful that he has provided me with enormous academic freewill to explore my ideas during my study, meanwhile constantly keeping me on track.

In addition, I wish to acknowledge the Malaysian Ministry of Higher Education and Universiti Kuala Lumpur for providing financial assistance for me to conduct my PhD study for the past four years.

Furthermore, I wish to express my very deep gratitude to my family members, for their patience in providing me unfailing support and continuous encouragement throughout my studies.

Finally, I would like to thank the technicians and staff of the School of Electrical and Electronic Engineering, especially, Mr. Jamaluddin Che Amat for giving me access to the school laboratory and research facilities.

## TABLE OF CONTENTS

	<b>Page</b>
<b>ACKNOWLEDGEMENT</b>	ii
<b>TABLE OF CONTENTS</b>	iii
<b>LIST OF TABLES</b>	viii
<b>LIST OF FIGURES</b>	x
<b>LIST OF ABBREVIATIONS</b>	xv
<b>LIST OF SYMBOLS</b>	xvii
<b>ABSTRAK</b>	xviii
<b>ABSTRACT</b>	xx
<b>CHAPTER ONE: INTRODUCTION</b>	
1.1 Research Background	1
1.2 Problem Statement	5
1.3 Research Objectives	6
1.4 Research Scope	7
1.5 Research Contributions	9

1.6	Thesis Outlines	10
-----	-----------------	----

## **CHAPTER TWO: LITERATURE REVIEW**

2.1	Introduction	12
2.2	Topology of Permanent Magnet Synchronous Machines	12
2.3	Output Torque	18
2.4	Minimization of Torque Ripple	18
2.5	Modelling of Permanent Magnet Synchronous Machines	29
	2.5.1 Analytical Sub-Domain Technique	29
2.6	Optimization in the Design of Electric Machines	32
	2.6.1 Optimization Classification	33
	2.6.2 Recent Studies on PMSM Optimization	35
	2.6.3 Multi-Objective Differential Evolution	40
2.7	Summary	42

## **CHAPTER THREE: METHODOLOGY**

3.1	Introduction	44
3.2	Motor Parameters and Sizing Equations	47
3.3	Configuration of Motor Windings	56
3.3.1	Pitch Factor in Motor Windings	58
3.3.2	Distribution Factor in Motor Windings	60
3.4	Analytical Sub-Domain Model	62
3.4.1	Magnetic Flux Density for Slotless PMSM	62
3.4.2	Complex Relative Permeance Function	80
3.4.3	Magnetic Flux Density for Slotted PMSM	92
3.5	Open-Circuit Condition	94
3.5.1	Phase Back-EMF	94
3.5.2	Cogging Torque	95
3.6	On-Load Condition	95
3.6.1	Current-Sheet Model	96
3.6.2	Armature Reaction Field Distributions	104

3.6.3	Output Power	112
3.6.4	Output Torque	113
3.6.5	Efficiency	113
3.7	Initial Design of PMSM	115
3.8	Optimization Technique	117
3.8.1	Optimized Parameters	117
3.8.2	Configuration of Optimization Technique Parameters	119
3.8.3	Multi-Objective Function	125
3.9	Summary	127
 <b>CHAPTER FOUR: RESULTS AND DISCUSSION</b>		
4.1	Introduction	128
4.2	Optimization Output	128
4.3	Optimized Design of PMSM	139
4.4	Air Gap Magnetic Flux Density for Slotless PMSM	143
4.5	Complex Relative Permeance Function	145

4.6	Air Gap Magnetic Flux Density for Slotted PMSM	146
4.7	Phase Back-EMF	152
4.8	Line-Line Back-EMF	154
4.9	Cogging Torque	156
4.10	Output Power	158
4.11	Output Torque	159
4.12	Cogging Torque Minimization using Skewing Method	162
4.13	Summary	170

## **CHAPTER FIVE: CONCLUSIONS AND RECOMMENDATIONS**

5.1	Conclusions	172
5.2	Recommendations for Future Work	175

<b>REFERENCES</b>	176
-------------------	-----

## **LIST OF PUBLICATIONS**



## LIST OF TABLES

		<b>Page</b>
Table 2.1	Pitch factor, winding factor, and distribution factor for PMSM.	15
Table 2.2	Slot/pole combination for 3-phase PMSM.	17
Table 2.3	Coil span for different slot/pole ratios.	17
Table 2.4	LCM and GCD for different slots with same poles in PMSMs.	22
Table 2.5	Recent studies on PMSM optimization.	37
Table 3.1	Parameters of initial PMSMs design.	118
Table 3.2	Performance of the initial PMSM design (by analytical technique).	117
Table 3.3	Maximum and minimum limits of PMSM parameters.	118
Table 3.4	ASGA optimization setting.	120
Table 3.5	ASPSO optimization setting.	121
Table 3.6	Selection values of $C_1$ , $C_2$ , $W_{max}$ , and $W_{min}$ for 6-slot/4-pole PMSM.	122
Table 3.7	Selection values of $C_1$ , $C_2$ , $W_{max}$ , and $W_{min}$ for 15-slot/10-pole PMSM.	123
Table 3.8	ASDEA optimization setting.	125
Table 3.9	Selection values of $F$ and $C_r$ for 6-slot/4-pole PMSM.	125
Table 3.10	Selection values of $F$ and $C_r$ for 15-slot/10-pole PMSM.	125
Table 4.1	ASGA results for 6-slot/4-pole PMSM.	132
Table 4.2	ASPSO results for 6-slot/4-pole PMSM.	134
Table 4.3	ASDEA results for 6-slot/4-pole PMSM.	135
Table 4.4	ASGA results for 15-slot/10-pole PMSM.	137
Table 4.5	ASPSO results for 15-slot/10-pole PMSM.	138
Table 4.6	ASDEA results for 15-slot/10-pole PMSM.	139
Table 4.7	Comparison of optimized parameters for 6-slot/4-pole PMSM.	140
Table 4.8	Comparison of optimized parameters for 15-slot/10-pole PMSM.	141

Table 4.9	Harmonics components of phase back-emf for PMSM before and after optimization.	153
Table 4.10	Harmonics components of line-line back-emf for PMSM before and after optimization.	155
Table 4.11	PMSMs performance after applying the three-step rotor skew.	163

## LIST OF FIGURES

		Page
Figure 1.1	Primary energy demand.	2
Figure 1.2	Shares of total power generation.	2
Figure 1.3	Primary energy consumption by the end-user sector.	3
Figure 1.4	Electric car usage.	3
Figure 1.5	Cumulative distribution of different electric machine technologies in EVs and HEVs from 1884 until 2016.	4
Figure 2.1	Internal rotor type for PMSM.	13
Figure 2.2	Winding type for PMSM.	14
Figure 2.3	Magnetization pattern and it's radial and tangential components.	16
Figure 2.4	Constant and periodic components of the torque.	18
Figure 2.5	Slotless PM motor configurations.	19
Figure 2.6	Different stator slot shapes.	21
Figure 2.7	Plug-in teeth.	21
Figure 2.8	Static torque for 12-slot/10-pole PMSM with unequal tooth width, alternate teeth wound, and all teeth wound.	21
Figure 2.9	Cogging torque for 20 poles motors with 60, 48, and 24 slots.	22
Figure 2.10	Different magnet shape for PMSM.	23
Figure 2.11	Cogging torque of 18-slot/12-pole PMSM for various PM offset.	23
Figure 2.12	Magnet sine shaping.	24
Figure 2.13	Magnet sine shaping with 3 <sup>rd</sup> harmonics.	24
Figure 2.14	Cogging torque for different magnet shaping.	25
Figure 2.15	(a) Initial shape of the permanent magnet. (b) After reshaping the edges.	25
Figure 2.16	Initial and modified cogging torque after reshaping the magnets.	26
Figure 2.17	Three-step magnet skew.	27
Figure 2.18	Cogging torque reduction after applying three-step rotor skew.	27
Figure 2.19	Rotor with two segments of permanent magnets.	28
Figure 2.20	Phase back-emf waveforms of 9-slot/10-pole PMSM with radial magnetization RM, parallel magnetization PaM, and ideal Halbach IH.	28

Figure 2.21	PMSM sub-domain.	31
Figure 3.1	Research framework.	44
Figure 3.2	Research design flowchart.	46
Figure 3.3	2-D design of slotted PMSM.	47
Figure 3.4	Magnetic flux flows in the air gap and stator tooth.	48
Figure 3.5	Non-oriented electrical steel (35JNE250) B-H curve.	50
Figure 3.6	Magnetic flux entering the stator yoke.	51
Figure 3.7	Stator tooth pole shape for slotted PMSM.	52
Figure 3.8	Stator slot depth.	53
Figure 3.9	Slot area for concentrated winding.	54
Figure 3.10	Rotor yoke height for PMSM.	55
Figure 3.11	Half of the stator pole.	56
Figure 3.12	Allocation of phase windings and magnet arrangement.	57
Figure 3.13	Formulation of pitch factor for the 6-slot/4-pole motor.	58
Figure 3.14	Coil mmf vectors and selection of coils per phase in 6-slot/4-pole PMSM.	61
Figure 3.15	Coil mmf vectors and selection of coils per phase in 15-slot/10-pole PMSM.	61
Figure 3.16	The boundary around the magnet and air gap regions.	65
Figure 3.17	Single magnet segment per magnetic pole.	66
Figure 3.18	Single slot infinitely deep slot opening in the S-plane.	81
Figure 3.19	Slot opening in the Z-plane.	82
Figure 3.20	Slot opening in the Z-plane with marked values of $w$ at the corner points.	83
Figure 3.21	Slot opening in the W-plane.	83
Figure 3.22	Slot opening in the T-plane.	85
Figure 3.23	Slot opening in the K-plane.	87
Figure 3.24	(a) Distributed current sheet model of a single conductor in slots. (b) Current sheet profile of a single conductor in slots.	96
Figure 3.25	(a) Distributed current sheet model of a single coil in slots. (b) Current sheet profile of a single coil in slots.	99
Figure 3.26	Air gap region boundary.	105
Figure 3.27	The end winding for PMSM.	114
Figure 3.28	2-D diagram of initial design for 6-slot/4-pole PMSM.	115
Figure 3.29	2-D diagram of initial design for 15-slot/10-pole PMSM.	116

Figure 3.30	2-D design of the selected five machine parameters to be optimized in PMSM.	118
Figure 3.31	Genetic Algorithm flowchart.	120
Figure 3.32	Particle Swarm Optimization flowchart.	122
Figure 3.33	Differential Evolution flowchart.	124
Figure 4.1	Scatter diagram for 6-slot/4-pole PMSM (Output torque and Efficiency versus Phase back-EMF THD <sub>v</sub> ).	129
Figure 4.2	Scatter diagram for 6-slot/4-pole PMSM (Output torque and Efficiency versus Cogging torque).	130
Figure 4.3	Scatter diagram for 15-slot/10-pole PMSM (Output torque and Efficiency versus Phase back-EMF THD <sub>v</sub> ).	131
Figure 4.4	Scatter diagram for 15-slot/10-pole PMSM (Output torque and Efficiency versus Cogging torque).	132
Figure 4.5	Process flow for searching the best data.	133
Figure 4.6	2-D diagram of optimized design for 6-slot/4-pole PMSM.	142
Figure 4.7	2-D diagram of optimized design for 15-slot/10-pole PMSM.	143
Figure 4.8	Air gap magnetic flux density distribution for slotless 6-slot/4-pole PMSM.	144
Figure 4.9	Air gap magnetic flux density distribution for slotless 15-slot/10-pole PMSM.	144
Figure 4.10	Complex relative permeance function for 6-slot/4-pole PMSM.	145
Figure 4.11	Complex relative permeance function for 15-slot/10-pole PMSM.	146
Figure 4.12	Radial component of air gap magnetic flux density distribution for slotted 6-slot/4-pole PMSM.	147
Figure 4.13	Tangential component of air gap magnetic flux density distribution for slotted 6-slot/4-pole PMSM.	147
Figure 4.14	Magnetic flux density contour for 6-slot/4-pole PMSM before optimization.	148
Figure 4.15	Magnetic flux density contour for 6-slot/4-pole PMSM after optimization.	148
Figure 4.16	Radial component of air gap magnetic flux density distribution for slotted 15-slot/10-pole PMSM.	150
Figure 4.17	Tangential component of air gap magnetic flux density distribution for slotted 15-slot/10-pole PMSM.	150
Figure 4.18	Magnetic flux density contour for 15-slot/10-pole PMSM before	151

	optimization.	
Figure 4.19	Magnetic flux density contour for 15-slot/10-pole PMSM after optimization.	151
Figure 4.20	Phase back-EMF for 6-slot/4-pole PMSM before and after optimization.	152
Figure 4.21	Phase back-EMF for 15-slot/10-pole PMSM before and after optimization.	153
Figure 4.22	Line-line back-emf for 6-slot/4-pole PMSM before and after optimization.	154
Figure 4.23	Line-line back-emf for 15-slot/10-pole PMSM before and after optimization.	155
Figure 4.24	Cogging torque for 6-slot/4-pole PMSM before and after optimization.	157
Figure 4.25	Cogging torque for 15-slot/10-pole PMSM before and after optimization.	157
Figure 4.26	Output power for 6-slot/4-pole PMSM before and after optimization.	158
Figure 4.27	Output power for 15-slot/10-pole PMSM before and after optimization.	159
Figure 4.28	Output torque for 6-slot/4-pole PMSM before and after optimization.	160
Figure 4.29	Output torque for 15-slot/10-pole PMSM before and after optimization.	160
Figure 4.30	Torque ripple obtained from the summation of cogging torque (open circuit) with electromagnetic torque (on-load) for 6-slot/4-pole PMSM after optimization.	161
Figure 4.31	Torque ripple obtained from the summation of cogging torque (open circuit) with electromagnetic torque (on-load) for 15-slot/10-pole PMSM after optimization.	161
Figure 4.32	Cogging torque of 6-slot/4-pole PMSM before and after rotor skewing.	164
Figure 4.33	Phase back-EMF of 6-slot/4-pole PMSM before and after rotor skewing.	164
Figure 4.34	Line-line back-EMF of 6-slot/4-pole PMSM before and after rotor skewing.	165

Figure 4.35	Output torque of 6-slot/4-pole PMSM before and after rotor skewing.	165
Figure 4.36	Output power of 6-slot/4-pole PMSM before and after rotor skewing.	166
Figure 4.37	Cogging torque of 15-slot/10-pole PMSM before and after rotor skewing.	167
Figure 4.38	Phase back-EMF of 15-slot/10-pole PMSM before and after rotor skewing.	167
Figure 4.39	Line-line back-EMF of 15-slot/10-pole PMSM before and after rotor skewing.	168
Figure 4.40	Output torque of 15-slot/10-pole PMSM before and after rotor skewing.	168
Figure 4.41	Output power of 15-slot/10-pole PMSM before and after rotor skewing.	169

## LIST OF ABBREVIATIONS

2-D	2-Dimension
3-D	3-Dimension
ASD	Analytical Sub-Domain
ASDEA	Analytical Sub-Domain Differential Evolution Algorithm
ASGA	Analytical Sub-Domain Genetic Algorithm
ASPSO	Analytical Sub-Domain Particle Swarm Optimization
CRPF	Complex Relative Permeance Function
DE	Differential Evolution
EB	Error-Based Optimization Search
EV	Electric Vehicle
FEA	Finite Element Analyses
FEM	Finite Element Method
GA	Genetic Algorithm
GUI	Graphic User Interface
HEV	Hybrid Electric Vehicle
HJ	Hooke-Jeeves
IBB	Interval Branch and Bound Method
ICE	Internal Combustion Engine
IRN	Interior Reflective Newton Method
IPM	Inverse Problem Method
MEC	Magnetic Equivalent Circuit
MODE	Multi-objective Differential Evolution
MOGA	Multi-objective Genetic Algorithm



MOPSO	Multi-objective Particle Swarm Optimization
PMa-SynRG	Permanent Magnet-Assisted Synchronous Reluctance Generators
PMSM	Permanent Magnet Synchronous Machine
PSO	Particle Swarm Optimization
SA	Simulated Annealing
SAFOM	Sub-problem Approximation and First-Order Method
SUMT	Sequential Unconstrained Minimization Technique
toe	tonnes of equivalent

## LIST OF SYMBOLS

$\alpha_p$	Magnet-arc to pole-pitch ratio
$B_g$	Average air gap flux density
$B_{max}$	Maximum flux density of iron
$b_o$	Slot opening
$h_m$	Magnet height
$K_{dn}$	Distribution factor
$K_{pn}$	Pitch factor
$l_g$	Air gap length
$N_p$	Winding turn per phase
$R_r$	Rotor radius
$R_m$	Magnet radius
$R_{ph}$	Phase winding resistance
$R_{si}$	Stator inner radius
$R_{so}$	Stator outer radius
$\omega_f$	Electrical angular frequency
$\omega_m$	Rotor speed
$w_{sy}$	Stator yoke width
$w_{tb}$	Tooth body width
$w_{tt}$	Tooth tip height/tooth tang
$\mu_m$	Recoil permeability of the magnet
$\mu_0$	Permeability of free space
$\mu_r$	Relative recoil permeability

# **PENGOPTIMUMAN MESIN SEGERAK MAGNET KEKAL PECAHAN LUBANG ALUR MENGGUNAKAN MODEL ANALITIKA SUB-DOMAIN DAN EVOLUSI KEBEZAAN**

## **ABSTRAK**

Haluan industri pada masa ini memerlukan pereka menghasilkan mesin elektrik yang mempunyai prestasi yang baik dalam jangka masa yang pendek, tetapi pemodelan mesin segerak magnet kekal menggunakan kaedah unsur terhingga memerlukan pengiraan masa yang panjang dan setiap kali parameter mesin diubah, pereka perlu mereka semula rekaan yang baru dan ini sangat memakan masa. Model analitika sub-domain dapat mengatasi masalah ini kerana ia mempunyai masa pengiraan yang cepat dibandingkan dengan kaedah unsur terhingga (FEM) dan litar bersamaan magnet (MEC). Bagi mengurangkan masalah kerja berulang, model pengoptimuman diguna agar dapat menyelesaikan masalah ini. Tiga teknik pengoptimuman pelbagai objektif menggunakan model analitika sub-domain (ASD) dan algoritma evolusi kebezaan (DEA), model analitika sub-domain (ASD) dan pengoptimuman kawanan zarah (PSO), model analitika sub-domain (ASD) dan algoritma genetik (GA), untuk mesin segerak magnet kekal pecahan lubang alur (PMSM) telah dirumuskan, dikira, dan dioptimumkan. Kemudian, prestasi mesin segerak magnet kekal pecahan lubang alur (PMSM) yang telah dioptimumkan di sahkan menggunakan kaedah unsur terhingga (FEM) 2-D. Dua model tiga-fasa mesin segerak magnet kekal pecahan lubang alur di kaji iaitu 6-lubang alur/4-kutub dan 15-lubang alur/10-kutub di mana ketebalan magnet, panjang jurang udara, nisbah lekuk magnet terhadap kutub-padang, bukaan lubang alur, dan jejari dalaman stator adalah antara parameter mesin yang dipilih untuk dioptimumkan. Fungsi objektif bagi

model pengoptimuman adalah: untuk mendapatkan getaran tork yang rendah, untuk mendapatkan gangguan herotan harmonik yang rendah dalam fasa voltan aruhan, untuk mendapatkan pengeluaran tork yang tinggi, dan untuk mendapatkan kecekapan yang tinggi. Berdasarkan kepada keputusan yang diperolehi, model analitika sub-domain algoritma evolusi kebezaan (ASDEA) mempunyai kebolehan pengoptimuman yang lebih baik dibandingkan dengan analitika sub-domain pengoptimuman kawanan zarah (ASPSO). ASDEA mempunyai 48.2 % lebih cepat masa pengiraan dari analitika sub-domain algoritma genetik (ASGA) bagi PMSM 6-lubang alur/4-kutub dan 71.5 % lebih cepat masa pengiraan dari analitika sub-domain algoritma genetik (ASGA) bagi PMSM 15-lubang alur/10-kutub. Mesin segerak magnet kekal 6-lubang alur/4-kutub yang telah dioptimumkan mempunyai kecekapan 95.5 %, pengeluaran tork 0.5491 Nm, pengeluaran kuasa 86.3 W, gangguan herotan harmonik dalam fasa voltan aruhan 9.9 %, dan riak tork 0.1566 Nm. Manakala mesin segerak magnet kekal 15-lubang alur/10-kutub yang telah dioptimumkan mempunyai kecekapan 93.71 %, pengeluaran tork 4.72 Nm, pengeluaran kuasa 296.22 W, gangguan herotan harmonik dalam fasa voltan aruhan 5.39 %, dan riak tork 0.47 Nm. Getaran tork dikurangkan lagi apabila rotor mesin segerak magnet kekal yang telah dioptimumkan dicondongkan dengan sudut condongan yang dipilih. Mesin segerak magnet kekal 6-lubang alur/4-kutub yang telah dioptimumkan dicondongkan dengan 30° mech. menghasilkan getaran tork 4.9 mNm. Manakala mesin segerak magnet kekal 15-lubang alur/10-kutub yang telah dioptimumkan dicondongkan dengan 12° mech. menghasilkan getaran tork 7.7 mNm.

# **OPTIMIZATION OF FRACTIONAL-SLOT PERMANENT MAGNET SYNCHRONOUS MACHINES USING ANALYTICAL SUB-DOMAIN MODEL AND DIFFERENTIAL EVOLUTION**

## **ABSTRACT**

Today's industrial trend requires designers to build electric machines with shorter design time and to have better performance. However, the modelling of Permanent Magnet Synchronous Machine (PMSM) using Finite Element Method requires longer computational burden and each time machine parameters are changed, the designers need to build another new design and it is relatively time-consuming. Analytical Sub-Domain model is able to overcome this problem due to its faster computational time compared with Finite Element Method (FEM) and Magnetic Equivalent Circuit (MEC). In order to reduce the repetitive and redundancy works, the optimization tool is deployed to solve this problem. Three multi-objective optimizations based on Analytical Sub-Domain (ASD) and Differential Evolution Algorithm (DEA), Analytical Sub-Domain (ASD) and Particle Swarm Optimization (PSO), Analytical Sub-Domain (ASD) and Genetic Algorithm (GA), for fractional-slot Permanent Magnet Synchronous Machines (PMSM) are formulated, computed and optimized. Then, the optimized fractional-slot Permanent Magnet Synchronous Machine (PMSM) performance is validated using the 2-D Finite Element Method (FEM). Two three-phase fractional-slot PMSM models are studied i.e. 6-slot/4-pole and 15-slot/10-pole in which the magnet thickness, air gap length, magnet arc to pole-pitch ratio, slot opening, and stator inner radius are the selected machine parameters to be optimized. The objective functions of the optimization model are: to have the lowest cogging torque, to have the lowest total harmonics distortion of

phase back-emf, to have the highest output torque, and to have the highest efficiency. From the results obtained, the Analytical Sub-Domain Differential Evolution Algorithm (ASDEA) has better optimization technique capability compared with Analytical Sub-Domain Particle Swarm Optimization (ASPSO). ASDEA is 48.2 % faster computational time than Analytical Sub-Domain Genetic Algorithm (ASGA) for 6-slot/4-pole PMSM and 71.5 % faster computational time than ASGA for 15-slot/10 pole PMSM. The optimized 6-slot/4-pole PMSM design has 95.5 % efficiency, 0.5491 Nm output torque, 86.3 W output power, 9.9 % total harmonics distortion of phase back-emf, and 0.1566 Nm torque ripple. While the optimized 15-slot/10-pole PMSM has 93.71 % efficiency, 4.72 Nm output torque, 296.22 W output power, 5.39 % total harmonics distortion of phase back-emf, and 0.47 Nm torque ripple. The cogging torque is further minimized when the rotor of the optimized PMSM models is skewed with a selected skewing angle. The optimized 6-slot/4-pole PMSM is skewed with 30° mech. resulting 4.9 mNm cogging torque. While the optimized 15-slot/10-pole PMSM is skewed with 12° mech. resulting 7.7 mNm cogging torque.

# CHAPTER ONE

## INTRODUCTION

### 1.1 Research Background

The energy report released in June 2018 shows an important indication of energy production and demand that forecast until 2040 (BP Energy Economics, 2018). The primary energy demand is categorized into six types i.e. renewable, hydro, nuclear, coal, gas, and oil. The energy demand recorded from the year 1970 until 2010 has increased from 5 billion toe to 12 billion toe, and this trend is predicted to be increasing until the year 2040 to 17 billion toes of energy demand as illustrated in Figure 1.1. The shares of total power generation are projected to be declining almost for all primary energy generation accepts an increasing generation of renewable energy as shown in Figure 1.2. This is due to the reduction of natural energy resources i.e. coal, oil, gas, nuclear, and hydro. Tremendous research on renewable energy leads to the increasing generation of renewable energy, i.e. solar, wind, biomass, geothermal, and tidal wave. Solar power will be a potential renewable energy source for power generation industry since the energy data provided by Global Solar Atlas shows the huge area in the world that have a high photovoltaic electricity output ranging from 700 kWh/kWp to 2400 kWh/kWp (GLOBAL Solar ATLAS, 2019). The other renewable energy might not so popular since the technology to support them is not purely matured as compared to the solar

energy system. Even though solar energy is freely available, but it is fluctuated depending on the weather of the site.

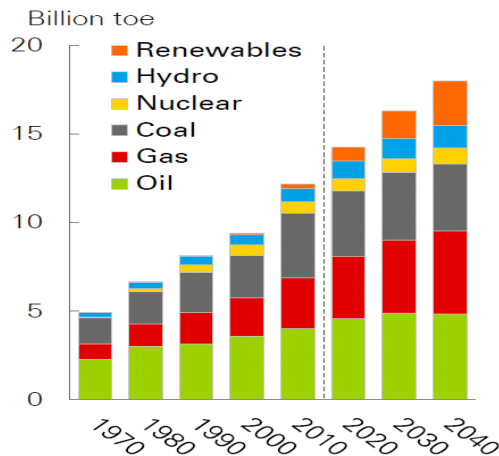


Figure 1.1: Primary energy demand (BP Energy Economics, 2018).

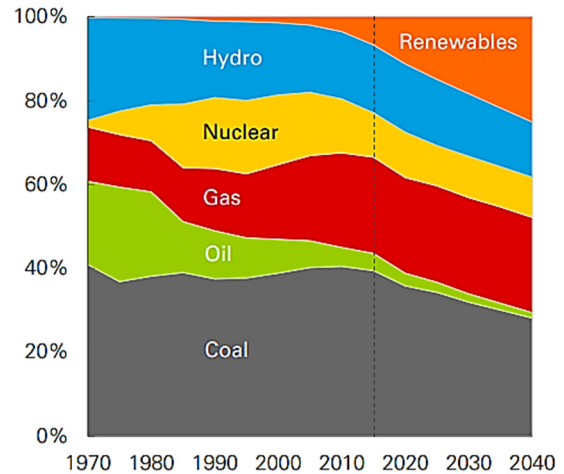


Figure 1.2: Shares of total power generation (BP Energy Economics, 2018).

Majority end users of energy consumption are from transport, industry, non-combusted, and building sectors. The energy consumption has increased since 1970 and projected to be the same trend until the year 2040 as shown in Figure 1.3. This is due to rapid development of country all over the world and increasing of the human population. New towns and industries are developed to cater to the increasing of the human population. Most of the new buildings have air handling units (AHUs) to regulate and circulate the air. AHUs have electric machines that are inserted in the blower to operate it. A high efficient electric machine can reduce the energy loss during operation and better AHU operation. Today industry employs automation in their production line, which uses many electric machines as the main system. This electric machine needs to operate accurately with high efficiency and minimal power



loss. In the transport sector, the majority end user is from a car that used an internal combustion engine (ICE). Due to the lower carbon emission requirement, the usage of ICE is going to reduce because ICE contributes to the higher carbon emission. As predicted in 2017, the electric vehicle (EV) usage projection shows a tremendous increase until the year 2035 and this trend will increase the EV usage to nearly 350 million of cars in the year 2040 as illustrated in Figure 1.4 (BP Energy Economics, 2018).

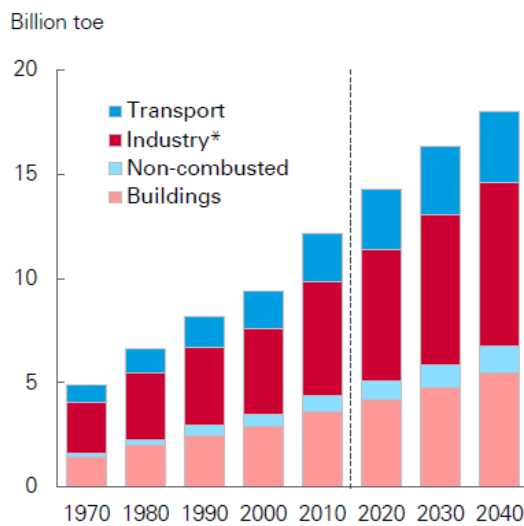


Figure 1.3: Primary energy consumption by end-user sector (BP Energy Economics, 2018).

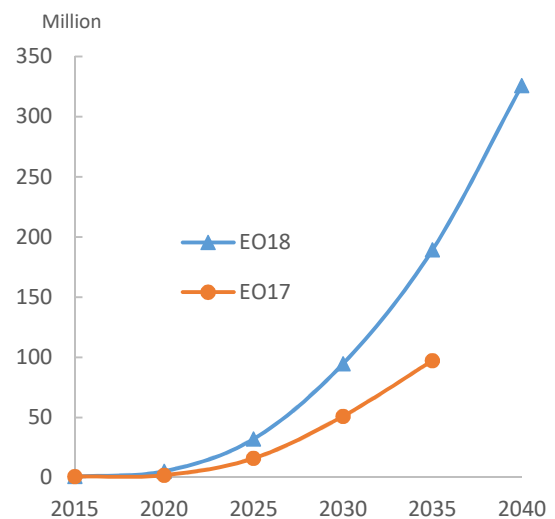


Figure 1.4: Electric car usage (BP Energy Economics, 2018).

The usage of permanent magnet synchronous machine (PMSM) in Electric Vehicles (EVs) and Hybrid Electric Vehicles (HEVs) is tremendously increasing as illustrated in Figure 1.5 and it has clearly become the famous candidate of electric machine in the near future as compared to other electric machine technologies (Bazzi, Liu and Fay, 2018). PMSM has a high torque density, high efficiency and

wide speed range of power capability compared to other types of electrical machines (Zhu and Howe, 2007). Nevertheless, PMSM still has few disadvantages such as high cogging torque, high torque ripples and eddy current losses (EL-Refai, 2010). Many types of research in designing and developing high-efficiency PMSM have been ongoing, starting from its modelling, parameters sizing, performances, and optimizations.

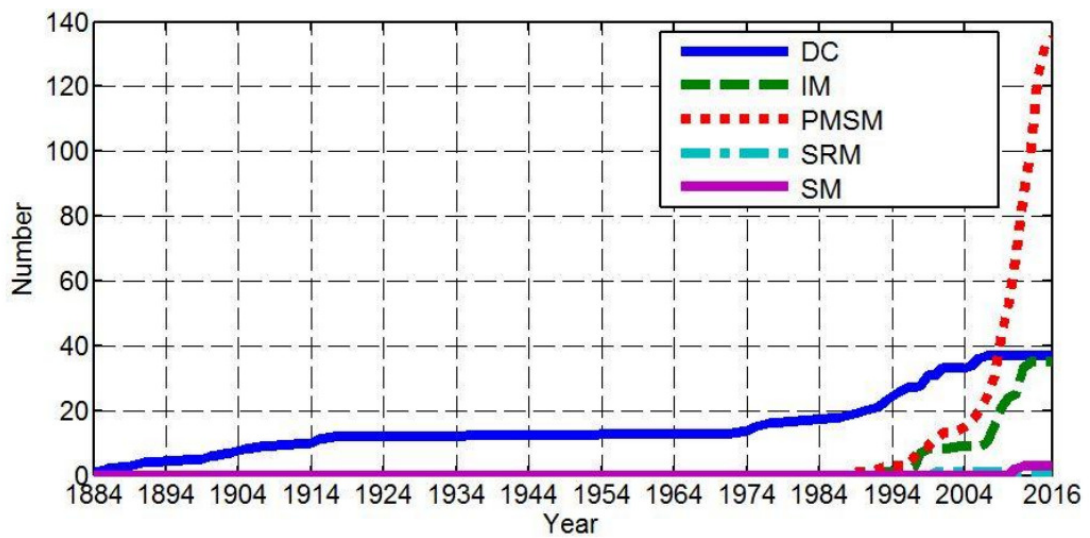


Figure 1.5: Cumulative distribution of different electric machine technologies in EVs and HEVs from 1884 until 2016 (Bazzi, Liu and Fay, 2018).

Since, PMSM is currently the best electric machine compared to others type of electric machine, then an optimization of PMSM is importance in order to obtained high performance electric machine with faster design time. So that the electric machine can be manufactured and be applied in the industry. This thesis present the development of a new multi-objective optimization technique using Analytical Sub-Domain model and Differential Evolution Algorithm (ASDEA). Other optimization techniques are developed i.e. Analytical Sub-Domain Genetic Algorithm (ASGA)

and Analytical Sub-Domain Particle Swarm Optimization (ASPSO). It is mainly to study the performance of those optimization techniques focusing on their computational time and optimization technique capability. All the results from the optimization techniques are validated using Finite Element Method (FEM).

## 1.2 Problem Statement

Accurate design of PMSM is usually performed using 2-D and 3-D finite element method (FEM), but it requires longer computational time compared to the analytical method (Lubin et al. 2011; Yilmaz & Krein 2008; Sizov et al. 2011). Even though the analytical method has certain limitations, it takes shorter computational time and provides good insights during the initial motor design stage (Zhu, Howe and Chan, 2002; Zarko, Ban and Lipo, 2009). Additionally, motor sizing equations can be used to select proper PMSM parameters (Rezal and Ishak, 2012). The performance of PMSM can be optimized using analytical sub-domain model by varying the motor parameters repetitively until achieving low cogging torque, low total harmonic distortions, high output torque, and high efficiency, but this method will take longer time and tedious because each motor parameter needs to be changed individually until reaching the targeted motor performance. In contrast, an optimization algorithm is able to solve this issue by searching the best values of machine parameters that yield the best output for certain objective functions (Duan, Harley and Habetler, 2009; Cvetkovski *et al.*, 2012; Šarac and Cvetkovski, 2014; Msaddek *et al.*, 2015; Guo *et al.*, 2016; Xue *et al.*, 2017).

Due to the computational burden, repetitive and redundancy work issues in FEM, the analytical sub-domain model is often preferred due to its lower computational time. A multi-objective differential evolution optimization can be used to optimize the PMSM design since it can reduce the redundancy work. This leads to high efficiency and high performance of PMSM design. This PhD study has a lot of significance, such as the design stage becomes faster with optimized PMSM parameters before moving to the fabrication stages.

Thus, the problem statements can be summarized as follows:

The FEM have a high computational time in order to design an electric machine.

1. Each time parameters of an electric machine is changed, then a new electric machine design need to be developed, creating a redundancy work and this lead to increasing of the design time.
2. Analytical Sub-Domain able to reduce the computational time, since Analytical Sub-Domain have the lowest computational time compared to FEM and Magnetic Equivalent Circuit (MEC).
3. Any optimization algorithm able to solve the issue of redundancy and repetitive work and the electric machine design time can be reduced.

### **1.3 Research Objectives**

The main aim of this study is to optimize the design of fractional-slot Permanent Magnet Synchronous Machines. The specific objectives of this research are as follows:

1. To develop a new multi-objective optimization technique based on Analytical Sub-Domain model and Differential Evolution Algorithm (ASDEA) for fractional-slot Permanent Magnet Synchronous Machine (PMSM);
2. To evaluate performance of Analytical Sub-Domain Differential Evolution Algorithm (ASDEA) with Analytical Sub-Domain Genetic Algorithm (ASGA) and Analytical Sub-Domain Particle Swarm Optimization (ASPSO) for fractional-slot Permanent Magnet Synchronous Machine (PMSM);
3. To optimize fractional-slot Permanent Magnet Synchronous Machine (PMSM) using Analytical Sub-Domain Differential Evolution Algorithm (ASDEA) and validate using the 2-D Finite Element Method (FEM).

#### **1.4 Research Scope**

This research only focuses on optimizing electrical performance of the fractional-slot, concentrated, non-overlapping winding surface-mounted Permanent Magnet Synchronous Machine (PMSM) because it has better efficiency, and lower cost compared to non-fractional-slot, distributed, overlapping winding. This is due to less copper and magnet volume used. Three-phase, 6-slot/4-pole and 15-slot/10-pole PMSMs are selected as the case design studies because these two designs have poor performance initially so that the PMSM performance can be easily visualized and compared before and after the optimization using Analytical Sub-Domain model and Differential Evolution Algorithm (ASDEA).

Initially, the PMSM parameters are identified using sizing equations after setting the fixed and variable values for machine parameters. Then, a semi-analytical sub-domain model is developed to determine the magnetic flux density in the air gap by considering only two regions i.e. magnet and air gap regions. Normally, analytical sub-domain applies full sub-domain in the model which consists of four regions i.e. magnet, air gap, slot opening, and winding slot. In order to model the slotting effect for the slotted PMSM, a Complex Relative Permeance Function (CRPF) is applied, where its output consists of the radial and tangential components of the magnetic flux density in the air gap. The cogging torque and phase back-emf are measured during the open-circuit condition. The output torque and efficiency are measured during the on-load condition. These initial machine parameters are saved and will be used as the benchmark for the optimization model.

Next, a multi-objective optimization model is applied to optimize PMSM based on the initial machine design obtained from the sizing equations and analytical sub-domain model. Three types of optimization techniques are applied i.e. Genetic Algorithm (GA), Particle Swarm Optimization (PSO), and Differential Evolution (DE) to obtain the optimized machine parameters that fulfil the objective functions set in the model. The computational time and optimization technique capability of the optimization techniques is analysed and compared. Four objective functions have been selected that are: (a) to have lowest cogging torque, (b) to have the lowest phase back-emf total harmonics distortion, (c) to have the highest output torque, and (d) to have the highest efficiency. Here, five machine parameters are selected as the optimization variables in the optimization model i.e. magnet thickness, air gap length, slot opening, magnet arc to pole-pitch ratio, and stator inner radius. Each of

them has minimum and maximum values so that the optimization model will run the iterations only within this constraint. The results of the optimization model are tabulated in the table and plotted in the graph using a Scatter diagram. The optimal solution for the optimized PMSM is selected by considering all the objective functions. Then optimized machine parameters, i.e. magnet thickness, air gap length, slot opening, magnet arc to pole-pitch ratio, and stator inner radius are then selected.

## **1.5 Research Contributions**

The majority of the previous research applied Analytical Sub-Domain (ASD) model that considers all four regions i.e. magnet, air gap, slot opening, and winding slot. This technique requires longer computational time since it has longer equations to compute and more regions to consider. Whereas in this research, only two regions are applied i.e. magnet and air gap regions. The slotting effect is modelled using Complex Relative Permeance Function (CRPF), resulting in a good agreement between analytical and finite element method. In the past ten years, most of the researches in optimizing Permanent Magnet Synchronous Machine applied Genetic Algorithm (GA) and Particle Swarm Optimization (PSO) in their optimization technique. Differential Evolution (DE) algorithm is able to optimize the electric machines to obtain the best machine performance by optimizing machine parameters for fractional-slot surface-mounted PMSM. In this research, new multi-objective optimization technique i.e. Analytical Sub-Domain model and Differential Evolution Algorithm (ASDEA) is formulated which has never been developed in optimizing fractional-slot surface-mounted Permanent Magnet Synchronous Machine (PMSM).

The performance of ASDEA is compared with other optimization techniques i.e. Analytical Sub-Domain Genetic Algorithm (ASGA) and Analytical Sub-Domain Particle Swarm Optimization (ASPSO). The results show that ASDEA has higher optimization technique capability compared to ASPSO (18 % for 6-slot/4-pole PMSM referring to Figure 4.2, and 62 % for 15-slot/10-pole PMSM referring to Figure 4.4) and faster computational time compared to ASGA (48.2 % for 6-slot/4-pole PMSM and 71.5 % for 15-slot/10-pole PMSM). The results shows a good agreement between analytical and Finite Element Method (FEM).

## **1.6 Thesis Outlines**

This thesis starts with Chapter One presents the introduction of the research by discussing the general overview of the research. A problem statement of the research is elaborated from the major concerns and then focused to the two important problems i.e. computational time, repetitive and redundancy works that are normally problems faced by the electric machine designers during the design process of PMSM before it goes to fabrication stage.

Chapter Two presents a literature review on the information related to electric machine technologies i.e. Permanent Magnet Synchronous Machine, its design stage, modelling of PMSM using analytical sub-domain model and sizing equations, and optimization of PMSM using Differential Evolution.

Chapter Three discusses the methodologies applied in this PhD research. Sizing equations are applied to determine machine dimension parameters. An



analytical sub-domain model is applied to model the air gap magnetic flux density, and from there the phase back-emf and cogging torque can be calculated analytically during open-circuit condition. During the on-load condition, the machine output torque, and efficiency can be investigated. Only two regions are considered in modelling the PMSM i.e. magnet and air gap regions. A Complex Relative Permeance Function (CRPF) is added in the analytical sub-domain model to include the slotting effects. The DE algorithm is used to optimize the PMSM after selecting certain objective functions and chosen machine variables to be optimized. Three optimization models are applied i.e. GA, PSO, and DE to compare the performance for each optimization model.

Next, the research findings and discussions are presented in Chapter Four. The optimization results from GA, PSO, and DE are tabulated in the table and plotted in Scatter diagram. The optimization variables for each objective function are saved in the table and the best settings are selected as long as it fulfils the objective functions. The magnetic flux density distributions for three-phase, 6-slot/4-pole and 15-slot/10-pole PMSMs before and after optimization are plotted for slotless and slotted stators. The phase back-emf, cogging torque, output torque, and output power are also plotted and analysed. The analytical results are verified with finite element method.

Finally, the conclusion is presented in Chapter Five together with a few recommendations for future research work.

## **CHAPTER TWO**

### **LITERATURE REVIEW**

#### **2.1 Introduction**

This chapter describes the topology of Permanent Magnet Synchronous Machine (PMSM) starting from its rotor types; internal or external, magnet locations at the rotor; surface-mounted or internal, the magnetization of the permanent magnet; radial, parallel or Halbach, and winding types; concentrated or distributed. Next, the modelling technique for Permanent Magnet Synchronous Machine is categorized into three general methods; analytical sub-domain, magnetic equivalent circuit, and finite element method. Then, the optimization of the electric machine is discussed into three sub-topic i.e. optimization classifications, recent researches on PMSM optimization, and multi-objective Differential Evolution. Finally, this chapter is summarized to highlight the research gap and its opportunity.

#### **2.2 Topology of Permanent Magnet Synchronous Machines**

The design of PMSM can be divided into two important components i.e. rotor type and winding type. The rotor type can be an internal or external rotor, while the winding can be concentrated or distributed winding. There are commonly PMSM internal rotor types i.e. surface-mounted (SM-PMSM), inset surface-mounted (SI-PMSM), internal (I-PMSM), V-shaped internal (VI-PMSM), and radial internal (RI-

PMSM) as illustrated in Figure 2.1 (Finken, Hombitzer and Hameyer, 2010). Different internal rotor types will have different magnetic strength due to the magnet location in the rotor core. For analytical sub-domain model, the surface-mounted (SM-PMSM) internal rotor type is preferred due to assumptions considered for the infinite permeability of the rotor and stator iron in the design (Hannon, Sergeant and Dupré, 2014).

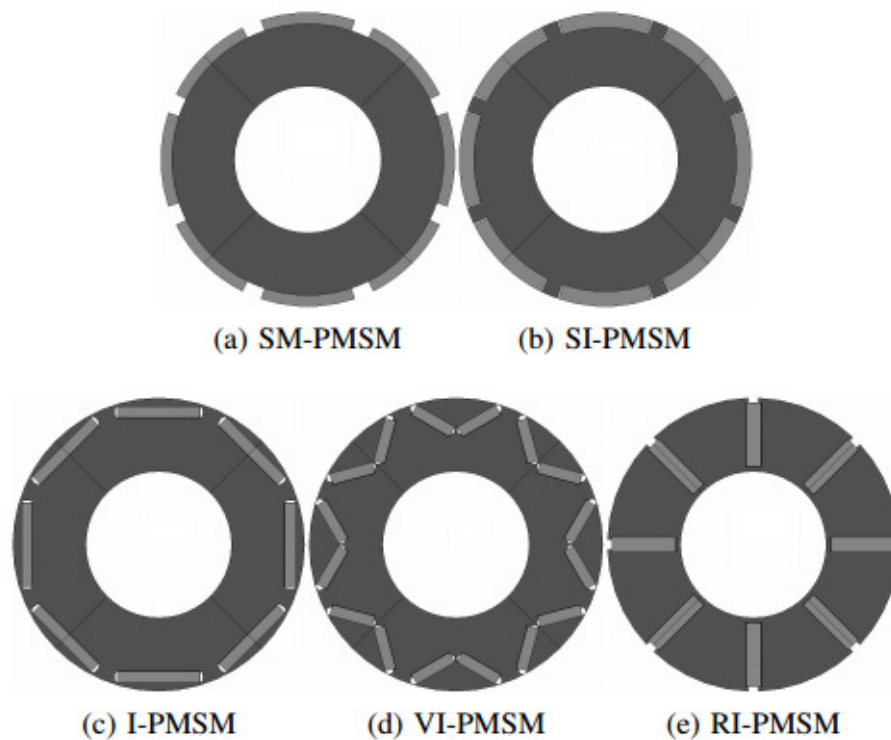


Figure 2.1: Internal rotor type of PMSM (Finken, Hombitzer and Hameyer, 2010).

PMSM with concentrated winding type, as illustrated in Figure 2.2(a), has better efficiency and lower cost due to less copper and magnetic volume used compared to distributed winding as shown in Figure 2.2(b) (Jussila *et al.*, 2007; Baek, Rahimian and Toliyat, 2009; Finken, Hombitzer and Hameyer, 2010).

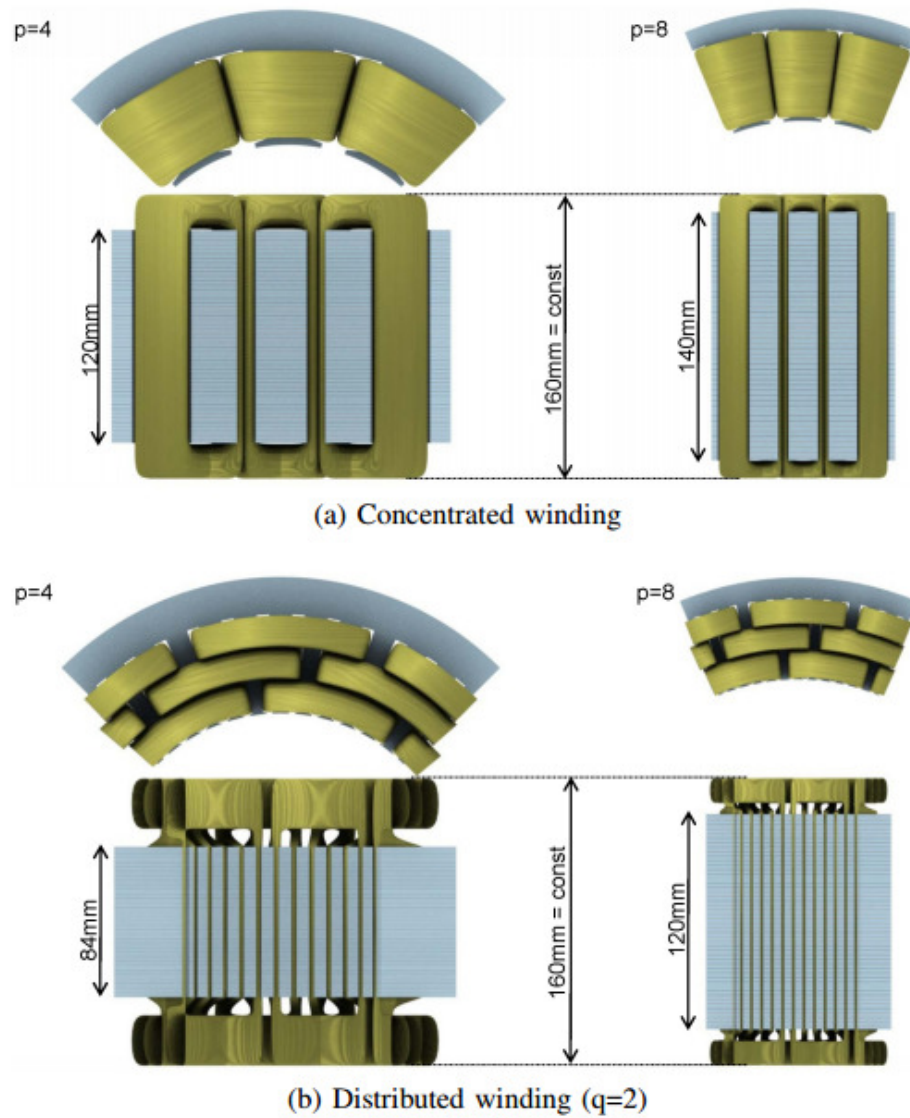


Figure 2.2: Winding type of PMSM (Finken, Hombitzer and Hameyer, 2010).

Each winding has its own pitch factor  $K_{pn}$ , distribution factor  $K_{dn}$ , and winding factor  $K_{dpn}$ , as shown in Table 2.1 (Ishak, Zhu and Howe, 2006). The winding factor  $K_{dpn}$  is obtained by multiplying pitch factor  $K_{pn}$  with distribution factor  $K_{dn}$ . Having an appropriate winding factor is important to eliminate the harmonics in phase back-emf waveform.

Table 2.1: Pitch factor, winding factor, and distribution factor for PMSM (Ishak, Zhu and Howe, 2006).

Slot/pole ( $N_s/2p$ )	Winding layout	$K_{pn}$	$K_{dn}$	$K_{dpn}$
6/4	All teeth ABCABC		1	$\sin\left(\frac{np\pi}{N_s}\right)$
	Alternate teeth ACB			
6/8	All teeth ACBACB			
	Alternate teeth ABC			
12/10	All teeth AA'B'CC'A'ABB'C' 'C	$\sin\left(\frac{np\pi}{N_s}\right)$	$\sin\left(\frac{np\pi}{N_s}\right)$	$\sin^2\left(\frac{np\pi}{N_s}\right)$
	Alternate teeth AB'CA'BC'		1	$\sin\left(\frac{np\pi}{N_s}\right)$
12/14	All teeth A'ACC'B'BAA'C'C BB'	$\sin\left(\frac{np\pi}{N_s}\right)$	$\sin\left(\frac{np\pi}{N_s}\right)$	$\sin^2\left(\frac{np\pi}{N_s}\right)$
	Alternate teeth AC'BA'CB'		1	$\sin\left(\frac{np\pi}{N_s}\right)$
18/16	All teeth A'AA'B'BB'C'CC' A'AA'B'BB'C'CC'		$\frac{1}{3}\left[1 - 2\cos\left(\frac{np2\pi}{N_s}\right)\right]$	$\frac{1}{3}\sin\left(\frac{np2\pi}{N_s}\right)\left[1 - 2\cos\left(\frac{np2\pi}{N_s}\right)\right]$
	Alternate teeth AB'B'CA'BC'C'			
18/20	All teeth A'AA'C'CC'BB'A' AA'C'CC'B'BB'			
	Alternate teeth AC'C'BA'A'CB'B'			

The rotor magnets can either be radial, parallel, or Halbach magnetization patterns (Rahideh and Korakianitis, 2012). The magnetization pattern and its components for radial, parallel, and Halbach permanent magnets are shown in Figure 2.3 respectively. Due to the absence of the tangential component, the radial magnetization pattern is the most preferred for the magnet in the analytical sub-domain model (Zhu, Howe and Chan, 2002). Magnetization patterns can greatly influence motor performance.

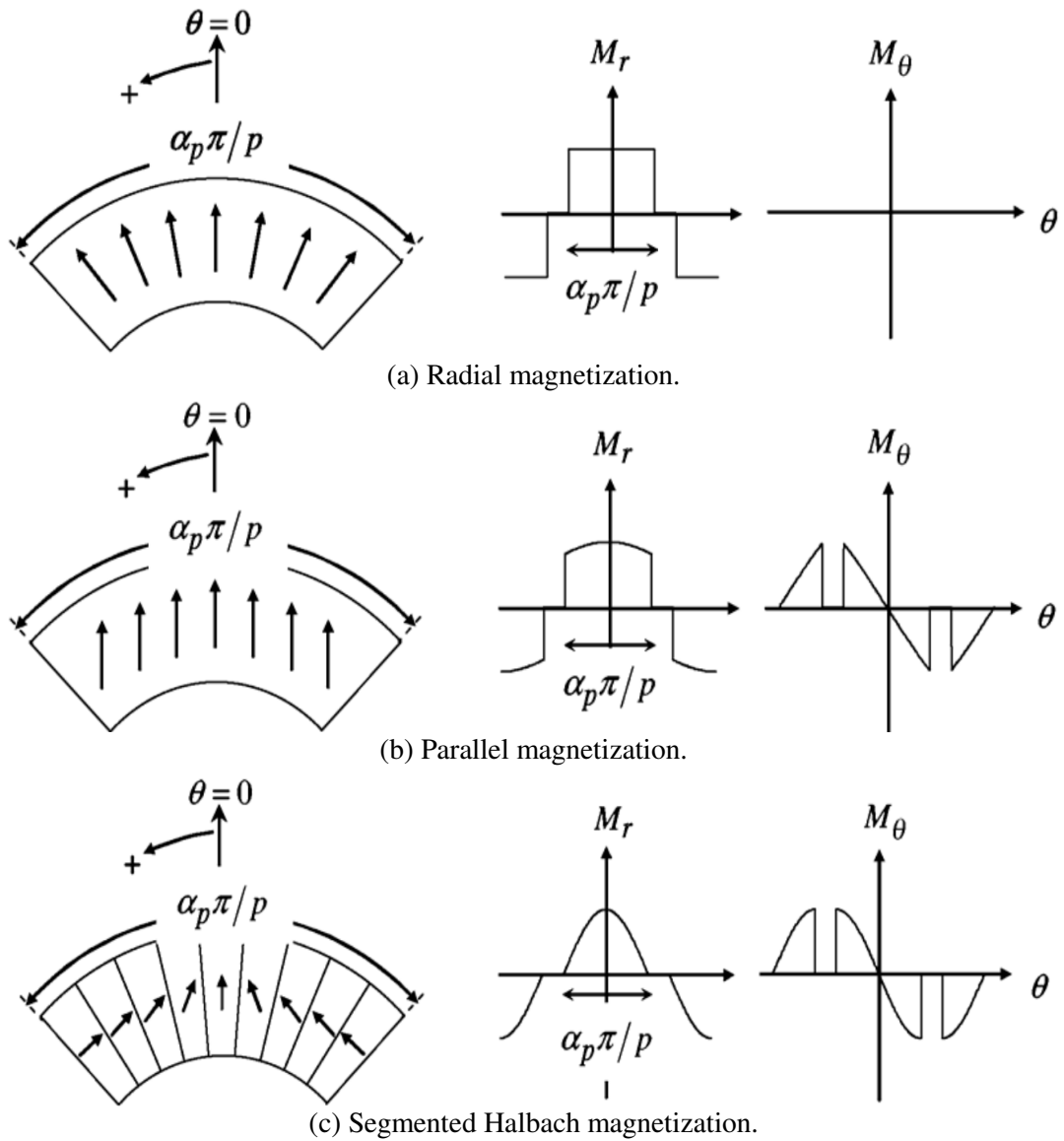


Figure 2.3: Magnetization pattern and its radial and tangential components (Rahideh and Korakianitis, 2012).

Another important criterion for machine design is the slot/pole combination. Table 2.2 shows the slot/pole combination for 3-phase PMSM. The coil span can be determined from the slot/pole combination. Table 2.3 shows the coil span for different slot/pole ratios.

Table 2.2: Slot/pole combination for 3-phase PMSM (Hendershot and Miller, 1994).

Slots	3	6	9	12	15	18	21	24	27	30	33	36	39	42	45	48
	2	2	2	2	2	2	2	2	2	2	2	2	2	2	2	2
	4	4	4	4	4	4	4	4	4	4	4	4	4	4	4	4
			6	8	10	6	8	10	6	8	8	8	8	8	6	8
			8	10		8	14	16	8	10	10	10	10	10	8	10
			12	18		12	16	20	10	20	14	12	14	14	10	14
						14			12	22	20	14	16	16	12	16
						16			18	26	22	16	26	26	14	20
Poles									20		26	22	28	28	16	32
									22		28	24	32	32	20	34
									24			26	34	34	28	38
												28			30	40
												30			32	
												32			34	
															38	
															40	

Table 2.3: Coil span for different slot/pole ratios (Hendershot and Miller, 1994).

Slot/pole	Coil span in slot pitches
0.75	1
1.125	1
1.5	1
2.25	2
3	3
3.75	3
4.5	4
5.25	5
6	6

PMSM has a fractional slot due to its slot/pole ratio. If the ratio is less than 1.5, then the PMSM will have fractional-slot windings since its coil are wound in a single-tooth (Ahmad *et al.*, 2012). Hence, end-winding is shorter and resulting in higher efficiency (Bianchi *et al.*, 2006; El-Refaie, 2010).

### 2.3 Output Torque

The instantaneous torque of an electrical motor as shown in Figure 2.4 has two parts i.e. average output torque  $T_0$  and periodic output torque  $T_r(\theta)$ . The periodic output torque can also be considered as torque ripple which exists due to the cogging torque and the harmonics contents of the magnetic flux density in the air gap (Gieras, 2010). The electric machine designer must design an electric machine with a minimal torque ripple and this can be done using few techniques as discussed in section 2.4.

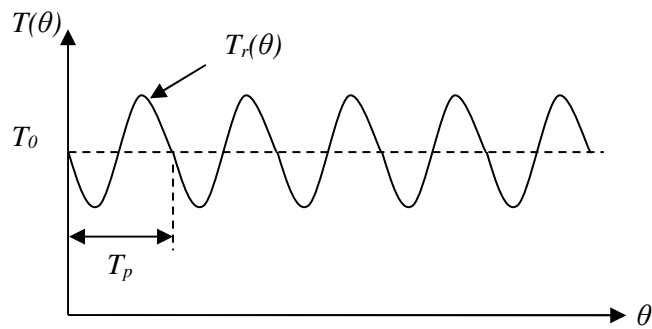


Figure 2.4: Constant and periodic components of the torque (Gieras, 2010).

### 2.4 Minimization of Torque Ripple

Torque ripple is the major concern of electric machine designer which if not handle carefully it will affect the electric machine performance. It also can disturbed the operation of the electric machine controllers. Adjusting the motor design and motor control can reduce the torque ripple. Skewed slots, slot shaping, slot/pole ratio, skewed rotor, shifted magnet segments, magnet width, magnetization pattern of PMs, and different size of tooth widths are few methods able to reduce the torque ripple



(Gieras, 2010). Control techniques include hysteresis current controller, space-vector PWM, and converter control strategy (Gopalakrishnan, Gopu and Gopalakrishnan, 2015; Bharatiraja *et al.*, 2017; Mohanraj and Sankaran, 2017)

The cogging torque can be reduced using slotless PMSM. The slotless PMSM can operate at high speed, compact design, high reliability, high efficiency, a minimum number of components, low cogging torque, and low total harmonics distortion THD (Gieras, 2014). An example of a slotless PM motor configuration is shown in Figure 2.5. It has two poles brushless PM motor with radial magnetization (Bianchi, Bolognani and Luise, 2005).

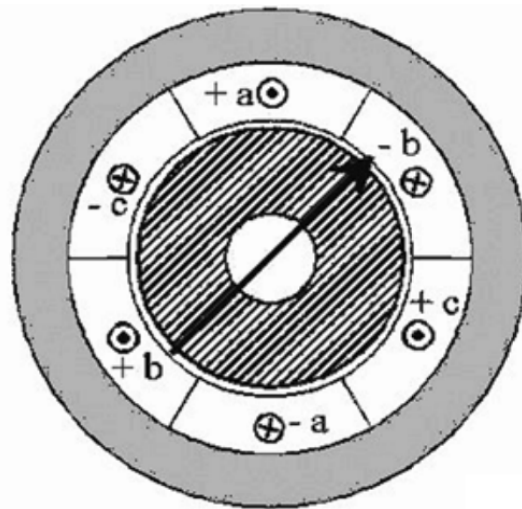


Figure 2.5: Slotless PM motor configuration (Bianchi, Bolognani and Luise, 2005).

The skewed rotor or stator can reduce the cogging torque (Levin *et al.*, 2013; Dhulipati *et al.*, 2017; Islam and Ortega, 2017). The back-emf slightly reduces when the rotor or stator is skewed, degrading the motor performance. Skewing the stator slots can embranch set of the stator winding, addition length of conductor and

decrease the useful area of the slot (Gieras, 2010; Levin *et al.*, 2013). Bifurcated slots, closed slots, pre-slots, and teeth with different width, slot opening width, additional auxiliary winding and slot shaping are other methods of reducing the cogging torque (Ishak, Zhu and Howe, 2005b; Guemes *et al.*, 2009; Abbaszadeh and Maroufian, 2014; G. Suresh Babu, T. Murali Krishna, 2015; Richnow, Gerling and Stenzel, 2015; Zhao *et al.*, 2016, 2017; Abdelmoula *et al.*, 2017; García-Gracia *et al.*, 2018). Figure 2.6 shows the different type of stator slot shapes. The cogging torque decreases with the decreases of the slot opening (Guemes *et al.*, 2009; Gieras, 2010). When designing closed slots, the bridge between the neighbouring teeth must be properly designed (Gieras, 2010; Abdelmoula *et al.*, 2017). Too thick bridge increases the stator slot leakage to an unacceptable level and too narrow a bridge can be ineffective due to high saturation (Gieras, 2010). Because closed slots can only have “sewed” coils, it is advisable to seal the slots by an enclosed internal sintered powder cylinder or split the stator yoke and the tooth-slot parts as shown in Figure 2.7 (Gieras, 2010; Richnow, Gerling and Stenzel, 2015). The performance of PMSM which have  $2p = N_s \pm 2$  and unequal tooth widths can offer useful performance benefits, in terms of a higher torque capability and reduced torque ripple (Ishak, Zhu and Howe, 2005b). Figure 2.8 shows the static torque for 12-slot/10-pole PMSM with unequal tooth widths, alternate teeth wound, and all teeth wound.

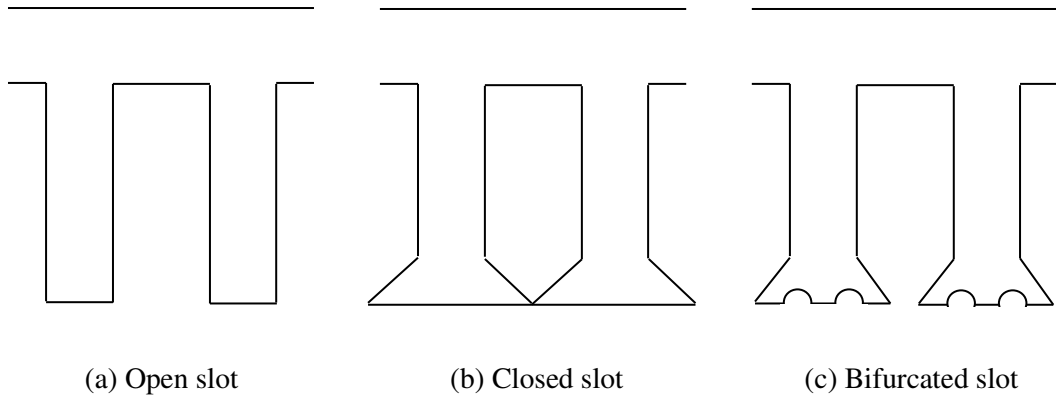


Figure 2.6: Different stator slot shapes.



Figure 2.7: Plug-in teeth (Richnow, Gerling and Stenzel, 2015).

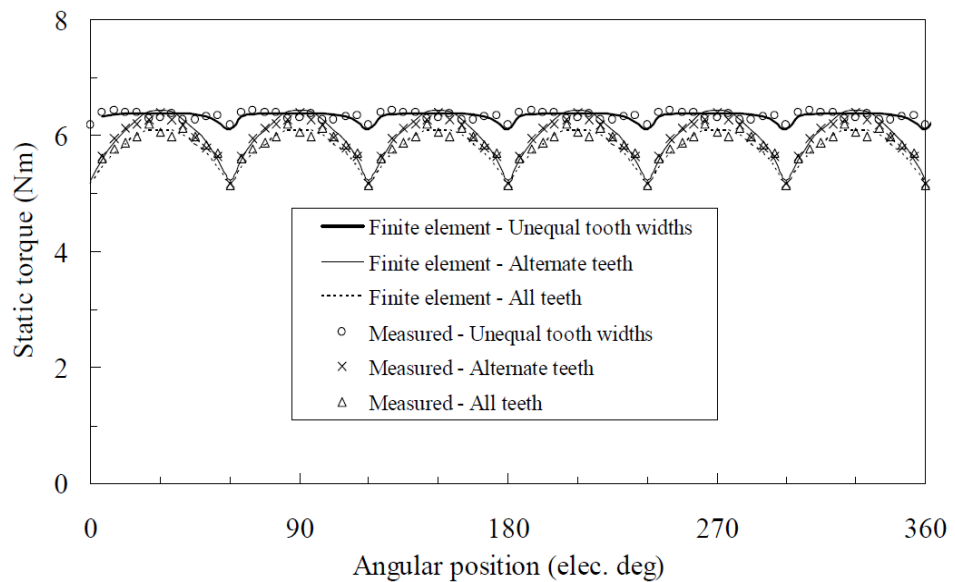


Figure 2.8: Static torque for 12-slot/10-pole PMSM with unequal tooth width, alternate teeth wound, and all teeth wound (Ishak, Zhu and Howe, 2005b).

The least common multiple LCM of the slot-pole number has a substantial influence on the cogging torque. As this number rise, the cogging torque reduces (Gieras, 2010; Güemes *et al.*, 2010; Dogan *et al.*, 2011). Similarly, the cogging torque rise as the greatest common divisor GCD of the slot-pole number rise (Gieras, 2010; Güemes *et al.*, 2010; Dogan *et al.*, 2011). The value for LCM and GCD for different slots with same poles PMSM is shown in Table 2.4. The 48-slot/20-pole PMSM has the highest LCM compared to other configurations resulting lowest cogging torque as shown in Figure 2.9.

Table 2.4: LCM and GCD for different slots with same poles PMSMs (Güemes *et al.*, 2010).

Slots	Poles	Slot pitch	Pole pitch	LCM	GCD
60	20	6°	18°	60	20
48	20	7.5°	18°	240	4
24	20	15°	18°	120	4

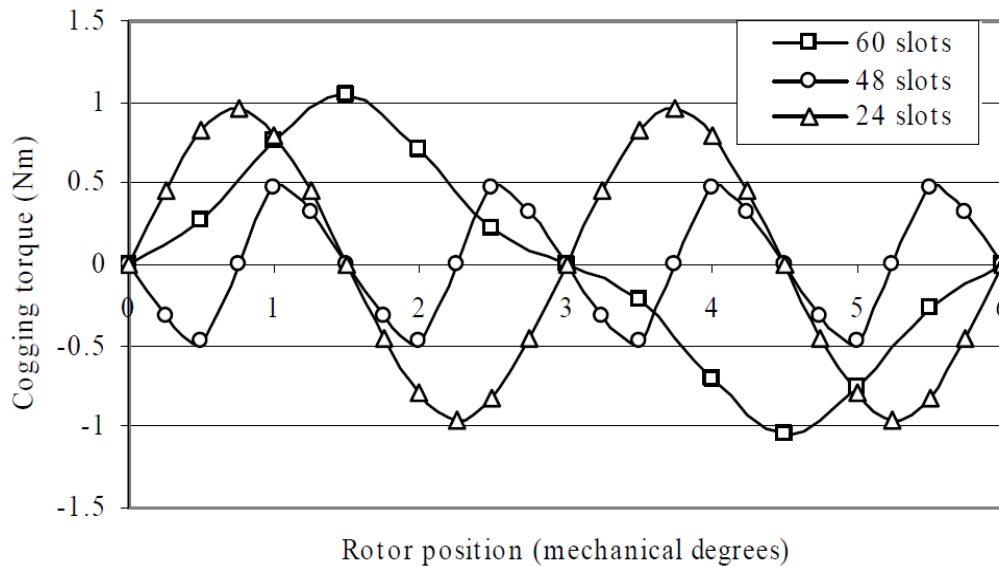


Figure 2.9: Cogging torque for 20 poles motors with 60, 48, and 24 slots (Güemes *et al.*, 2010).

Different magnet shapes of surface-mounted PM are shown in Figure 2.10. The bar shape PM produces more average torque compared to loaf and petal provided all other dimensions and parameters of the motor remain the same (Islam *et al.*, 2009). The torque ripple can be reduced by shaping the magnet pole (Upadhayay and Rajagopal, 2013). The cogging torque is reduced to minimal when the magnet pole is offset with 30 mm as shown in Figure 2.11.

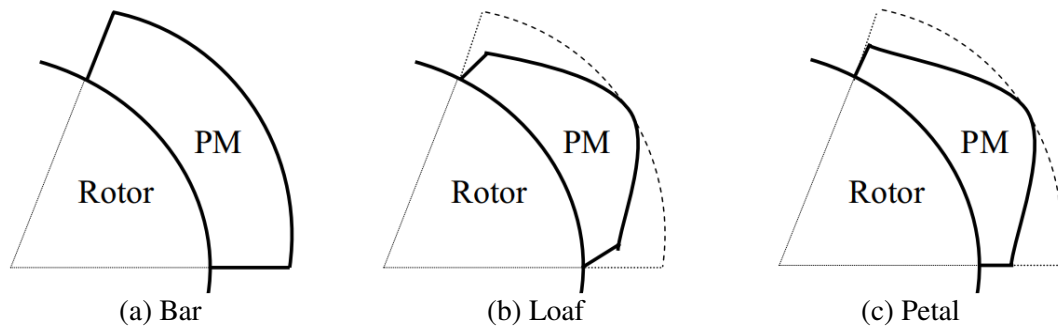


Figure 2.10: Different magnet shape for PMSM (Islam *et al.*, 2009).

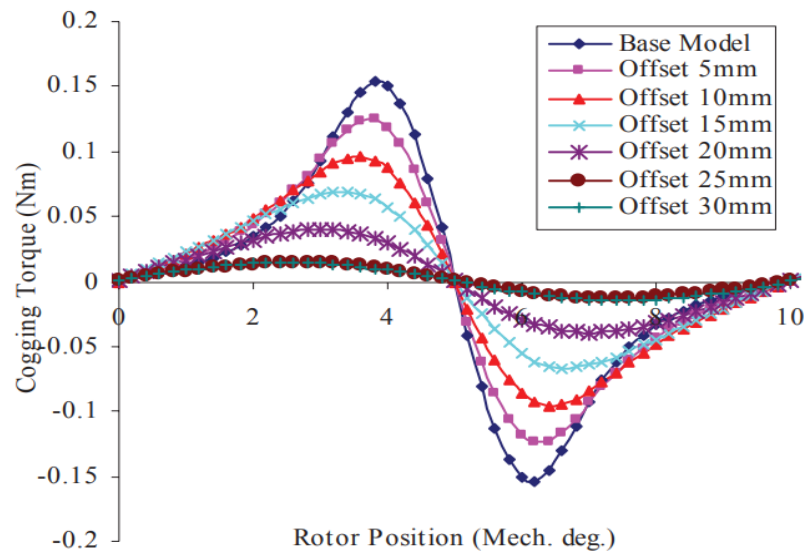


Figure 2.11: Cogging torque of 18-slot/12-pole PMSM for various PM offset (Upadhayay and Rajagopal, 2013).

Magnet sine shaping can also minimize torque ripple for sinusoidal air gap flux density. While magnet sine shaping with 3<sup>rd</sup> harmonic retains the 3<sup>rd</sup> harmonic of air gap flux density to increase the torque density (Lin *et al.*, 2015). Figures 2.12 and 2.13 show the magnet sine shaping without and with 3<sup>rd</sup> harmonic respectively.

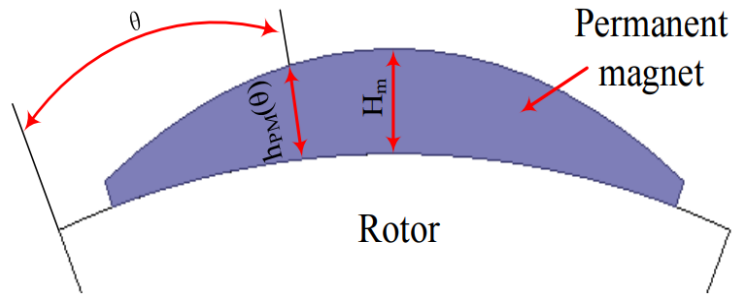


Figure 2.12: Magnet sine shaping (Lin *et al.*, 2015).

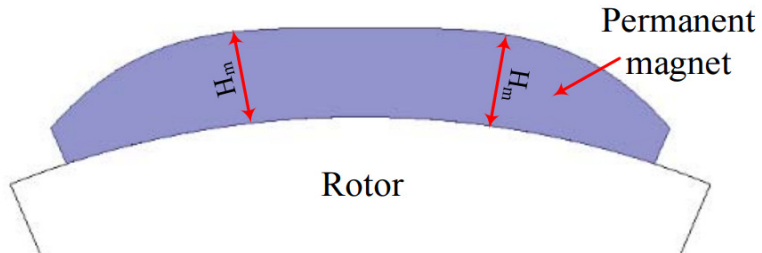


Figure 2.13: Magnet sine shaping with 3<sup>rd</sup> harmonic (Lin *et al.*, 2015).

The thickness of PM  $h_{PM}(\theta)$  with rotor position  $\theta$  in Figure 2.12 is

$$h_{PM}(\theta) = H_m \sin(p\theta) \quad (2.1)$$

and thickness of PM  $h_{PM}(\theta)$  with rotor position  $\theta$  in Figure 2.13 is

$$h_{PM}(\theta) = \frac{2\sqrt{3}}{3} H_m \left[ \sin(p\theta) + \frac{1}{6} \sin(3p\theta) \right] \quad (2.2)$$